Study of Optical Properties of MOCVD-Grown Rutile GeO₂ Films

Imteaz Rahaman^{1,*}, Anthony Bolda¹, Botong Li¹, Hunter D. Ellis¹, and Kai Fu^{1,*}

¹Department of Electrical and Computer Engineering, The University of Utah, Salt Lake City, UT 84112, USA

Abstract

Rutile germanium dioxide (r-GeO₂) is a promising ultra-wide bandgap (UWBG) semiconductor, offering a high theoretical Baliga figure of merit, potential for p-type doping, and favorable thermal and electrical properties. In this work, we present a comprehensive optical investigation of crystalline r-GeO₂ thin films grown on r-TiO₂ (001) substrates via metal-organic chemical vapor deposition (MOCVD). Cathodoluminescence (CL) spectroscopy reveals broad visible emissions with distinct peaks near 470 nm and 520 nm. CL mapping indicates enhanced emission intensity in regions with larger crystalline domains, highlighting the correlation between domain size and optical quality. X-ray photoelectron spectroscopy (XPS) confirms the presence of Ge⁴⁺ oxidation state and provides a bandgap estimation of ~4.75 eV based on valence band and secondary electron cutoff analysis. UV–Vis transmittance measurements show a sharp absorption edge near 250–260 nm, corresponding to an optical bandgap in the range of 4.81–5.0 eV. These findings offer valuable insights into the defect-related emission behavior and band-edge characteristics of r-GeO₂, reinforcing its potential for future applications in power electronics and deep-ultraviolet optoelectronic devices.

a) Author to whom correspondence should be addressed. Electronic mail: u1351894@utah.edu, kai.fu@utah.edu

The global demand for high-efficiency electronic, optoelectronic, and power devices has driven substantial interest in wide-bandgap (WBG, Eg≈3–4.5eV)¹ and ultrawide-bandgap (UWBG, Eg≥4.5eV)² semiconductors.² These materials offer advantages such as high electric

breakdown fields, wide transparency windows, and superior thermal stability, making them well-suited for next-generation technologies operating under extreme voltage, temperature, and radiation conditions.^{3–7} While SiC and GaN have become established in power conversion and RF applications, UWBG materials like AlN, β -Ga₂O₃, and diamond promise even greater performance by enabling more compact device architectures and higher power densities.^{8–11} In parallel, transparent semiconducting oxides (TSOs) with UWBGs such as Ga₂O₃ (α , β , and other polymorphs)^{12,13}, (Al_xGa_{1-x})₂O₃ (α and β)^{14,15}, MgGa₂O₄ (Eg=5 eV)¹⁶, ZnGa₂O₄(Eg=4.6 eV)¹⁷, or CuGa₂O₄ (Eg=4.5 eV)¹⁸ have garnered increasing attention due to their dual electronic and optical functionality, particularly for deep-ultraviolet (DUV) optoelectronic applications, including solar-blind photodetectors and UV-LEDs.

Among emerging UWBG TSOs, rutile germanium dioxide (r-GeO₂) has gained significant interest due to its unique combination of physical properties. The rutile phase exhibits a direct optical bandgap in the range of ~4.4–5.1 eV^{19–21}, high electron mobility [244 cm²/Vs ($^{\perp}$ C) and 377 cm²/V·s (($^{\parallel}$ C)]²², Baliga figure of merit 139.68 GW/cm⁻²²³ and thermal conductivity approaching ~58 W·m⁻¹·K⁻¹.²⁴ Favorable valence-band dispersion in r-GeO₂ supports theoretical predictions of ambipolar doping, and both theoretical and experimental studies indicate that group-III acceptors such as Ga, can enable p-type conduction—a significant advancement over the doping limitations typically encountered in current UWBG oxides.^{20,25} These characteristics position r-GeO₂ as a promising candidate for high-power and deep-UV optoelectronic devices. Various growth techniques have been employed to synthesize r-GeO₂, including top-seeded solution growth (TSSG)², Na₂O-based flux synthesis²⁶, and thin-film methods such as pulsed laser deposition (PLD)^{21,27,28}, mist chemical vapor deposition (mist-CVD)^{29,30}, molecular beam epitaxy (MBE)³¹, and metal-organic chemical vapor deposition (MOCVD)²³. However, achieving phase-pure, large-

area r-GeO₂ films with high crystallinity remains a challenge, particularly for scalable deposition platforms like MOCVD.²³ The optical properties of r-GeO₂ are sensitive to its crystalline quality and defect landscape. Photoluminescence (PL) studies have reported broad blue–green emission bands²⁸, typically associated with intrinsic or defect-related recombination. Shinde *et al.* observed PL peaks at 3.0 eV (415 nm) and 2.2 eV (560 nm) from microrod structures³², while Trukhin *et al.* attributed similar emissions to singlet-singlet and triplet-singlet transitions associated with oxygen-deficient centers³³. Synchrotron-based PL measurements have further identified peaks near 2.4 and 2.8 eV in PLD-grown films, underlining the role of defect states in emission characteristics.²⁸ Despite these advances, detailed correlations between film quality, surface morphology, defect-related optical features, and band-edge absorption, particularly for MOCVD-grown r-GeO₂, remain underexplored.

In this study, we present a comprehensive investigation of the optical properties of MOCVD-grown r-GeO₂ thin films. We combine structural and morphological analysis with cathodoluminescence (CL) spectroscopy, CL mapping intensity, X-ray photoelectron spectroscopy (XPS), and UV-Vis transmittance spectroscopy. By integrating these complementary techniques, we aim to clarify the relationship between crystalline quality, surface features, luminescence behavior, and optical bandgap. This work not only provides fundamental insights into the optical characteristics of r-GeO₂ films but also contributes to the broader development of this emerging UWBG semiconductor for next-generation optoelectronic and power device applications.

Undoped GeO₂ films were deposited using an Agilis MOCVD system (Agnitron Technology). Rutile TiO₂ (001) substrates were selected owing to their low lattice mismatch and favorable strain compatibility with GeO₂.^{29,34} The growth was carried out at 925 °C, employing a seed-driven

stepwise crystallization (SDSC) process.³⁵ The chamber pressure was maintained at 300 Torr during the initial 30 min \times 6 growth steps and reduced to 80 Torr for the remaining 30 min \times 12 steps. Tetraethylgermane (TEGe) and high-purity oxygen (O₂) served as the Ge and oxidant precursors, respectively, while argon (Ar) was used both as the carrier and shroud gas. The TEGe and O₂ flow rates were controlled at 1.35×10^{-5} mol/min and 8.94×10^{-2} mol/min, respectively. To ensure uniform film deposition, the susceptor was rotated at 300 RPM during growth. Prior to loading into the MOCVD chamber, the substrates underwent a piranha cleaning process (3:1 sulfuric acid to hydrogen peroxide), followed by sequential rinsing with acetone, isopropanol, and deionized water.

Figure 1 illustrates the surface morphology, crystallographic orientation, and microstructural quality of r-GeO₂ films grown on r-TiO₂ (001) substrates via MOCVD. The SEM image in **Figure 1a** reveals a faceted surface morphology with distinct grain boundaries and a uniform, well-aligned crystal orientation over a large area, indicating high-quality crystalline film growth. **Figure 1b** presents the 3D atomic force microscopy (AFM) topography, confirming the faceted nature of the surface with a peak-to-valley height variation of approximately 0.48 μ m across the scanned region (3.4 μ m × 3.2 μ m). AFM results support the SEM observation of surface roughness arising from faceted crystal growth. **Figure 1c** displays the ω –2 θ X-ray diffraction (XRD) pattern, where a sharp and intense r-GeO₂ (002) peak is observed alongside the r-TiO₂ (002) substrate peak, suggesting highly oriented, single-crystalline growth of r-GeO₂ along the [001] direction. To confirm the crystallinity at the atomic level, **Figure 1d** presents a high-resolution transmission electron microscopy (HRTEM) image of the r-GeO₂ film. Clear lattice fringes corresponding to the (-101) and (00-2) planes are observed with interplanar spacings of 0.161 Å and 0.271 Å.

respectively, which match well with rutile GeO₂. The inset fast Fourier transform (FFT) further confirms the high crystalline quality and absence of amorphous regions.

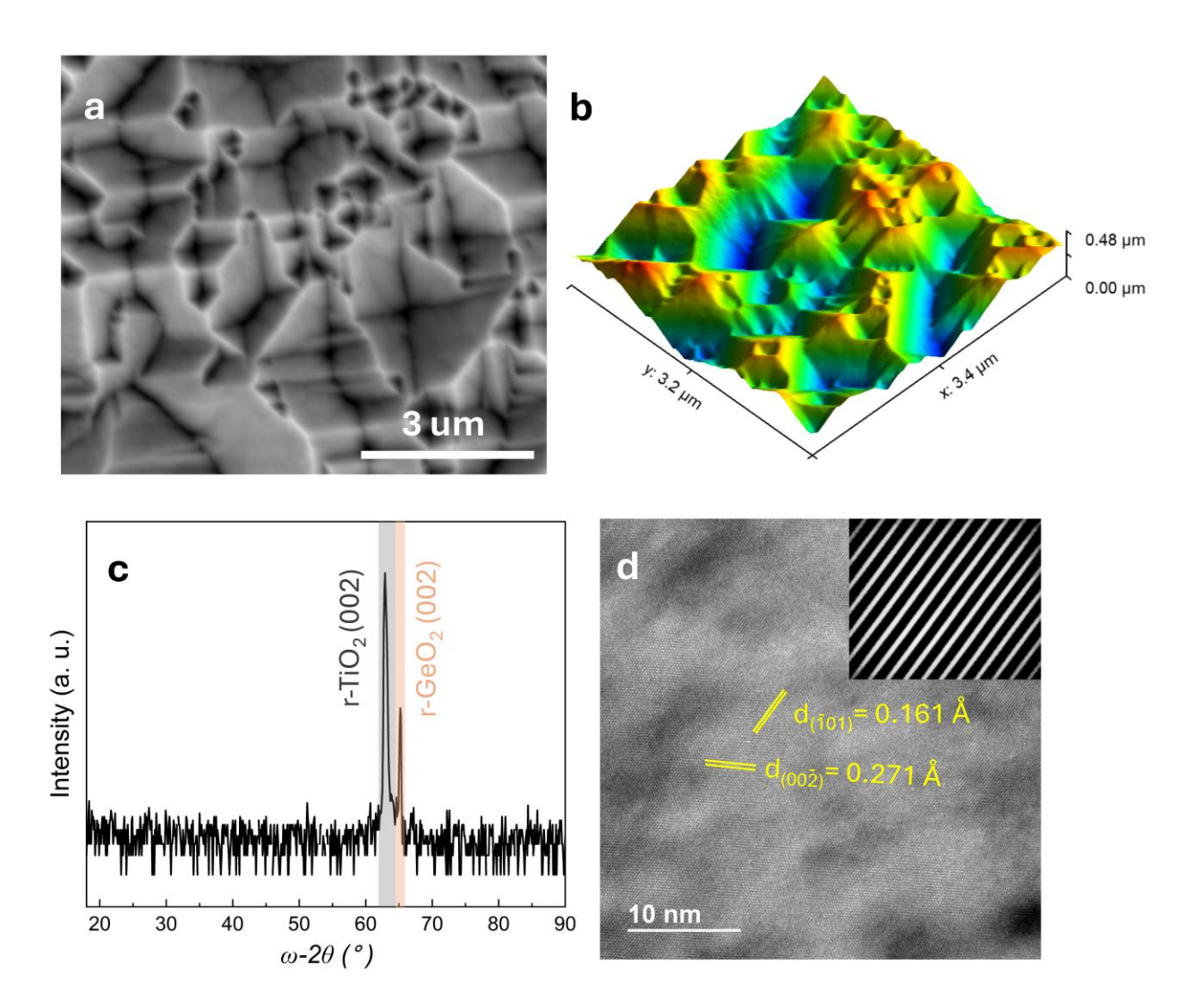


FIG. 1. Structural and morphological characterization of r-GeO₂ films grown on r-TiO₂ (001) by MOCVD. (a) SEM image showing faceted surface morphology. (b) 3D AFM topography confirming surface roughness due to faceting. (c) XRD pattern exhibiting sharp (002) peaks from both r-GeO₂ and the r-TiO₂ substrate, indicating single-crystalline growth. (d) HRTEM image showing clear lattice fringes and corresponding FFT, confirming high crystallinity.

Figure 2 presents a spatially resolved correlation between surface morphology and optical emission behavior across various regions of r-GeO₂ films, as examined by scanning electron

microscopy (SEM), cathodoluminescence (CL) mapping, and merged overlays. Each row (a–f) displays SEM images (left), CL intensity maps (middle), and merged images (right), with CL intensity visualized as red emission. Brighter red regions indicate stronger luminescence, whereas darker gray areas correspond to reduced optical activity.

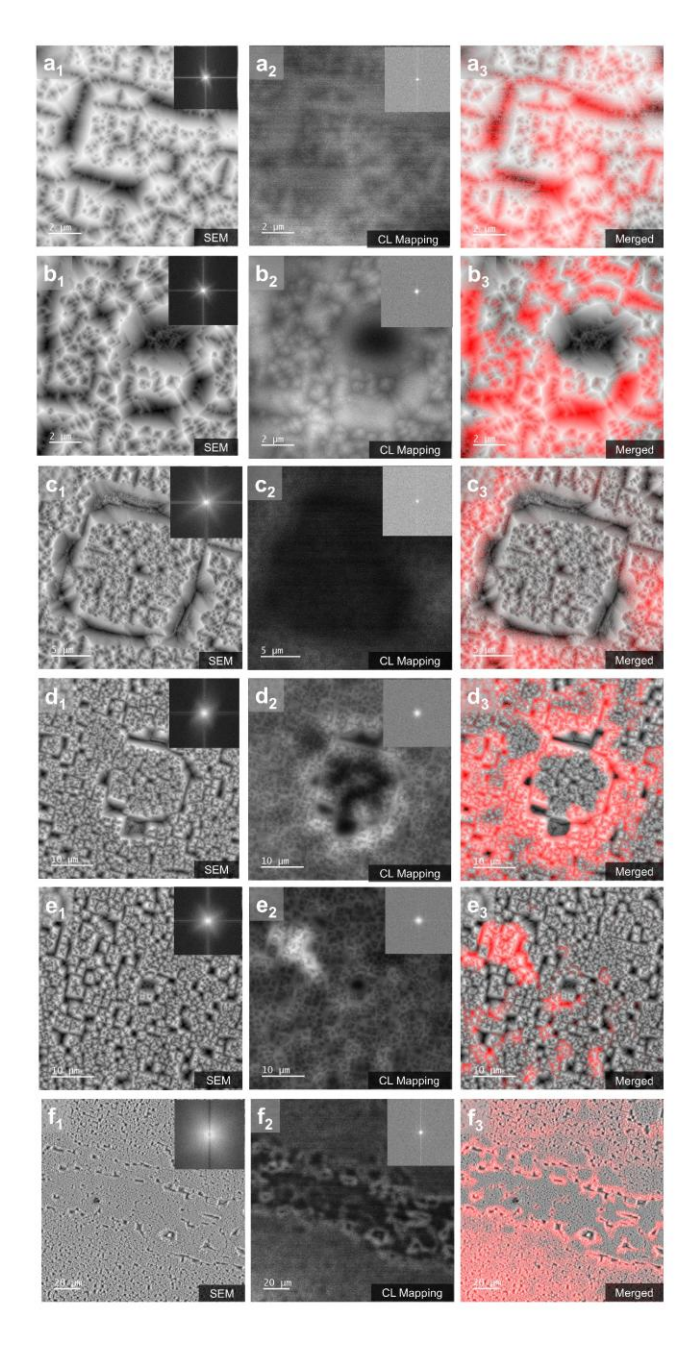


FIG. 2. Correlated SEM and CL mapping of r-GeO₂ films at different surface regions. Each row shows (left to right): SEM image, corresponding CL mapping, and merged overlay.

Strong CL emission is consistently observed from well-developed, faceted crystalline surfaces (a₁ and c₁), as shown in the merged panels (a₃ and c₃). These regions exhibit sharp geometrical facets and strong diffraction contrast in SEM, suggesting high crystalline quality and low defect density—favorable conditions for radiative recombination. In contrast, areas surrounding large surface depressions or valleys show markedly weaker CL response, particularly when accompanied by disordered morphologies (b₃ and d₃). These features are likely associated with strain accumulation, defect clustering, or local non-radiative recombination centers. Regions with rough nanoscale textures and small granular features (d₁–f₁) exhibit moderate to weak CL intensity (d₂–f₂), pointing toward enhanced surface recombination and defect-assisted quenching. Notably, the suppression of luminescence in these zones implies that small grains and high interface density adversely affect radiative efficiency. The observed trends remain consistent across varying magnifications (2–20 µm), reinforcing the conclusion that surface morphology exerts significant influence on local luminescent behavior in r-GeO₂ films.

Figure 3 presents the cathodoluminescence (CL) spectra of the underlying r-TiO₂ (001) substrate (Figure 3a) and the MOCVD-grown r-GeO₂ films (Figure 3b), measured at room temperature. The CL spectrum of the r-TiO₂ substrate reveals a broad emission profile comprising three deconvoluted peaks, labeled D_{T1}, D_{T2}, and D_{T3}, located at approximately 2.80 eV, 2.56 eV, and 2.10 eV, respectively. These features are consistent with defect-related transitions in rutile TiO₂, often attributed to oxygen vacancies and deep-level recombination pathways, as widely reported in the literature.^{36,37} Notably, D_{T1} is characteristic of blue emission commonly observed in both stoichiometric and reduced TiO₂, while the lower-energy peaks D_{T2} and D_{T3} likely arise from deeper trap states or recombination involving defect complexes.

In contrast, the r-GeO₂ film (Figure 3b) exhibits two dominant emission peaks, labeled D_{G1} and D_{G2} , centered around 470 nm $(2.64 \, \text{eV})^{38,39}$ and 520 nm $(2.38 \, \text{eV})^2$, respectively. These emissions fall within the blue–green spectral range and align with prior observations on r-GeO₂, often linked to intrinsic or defect-related luminescence centers.

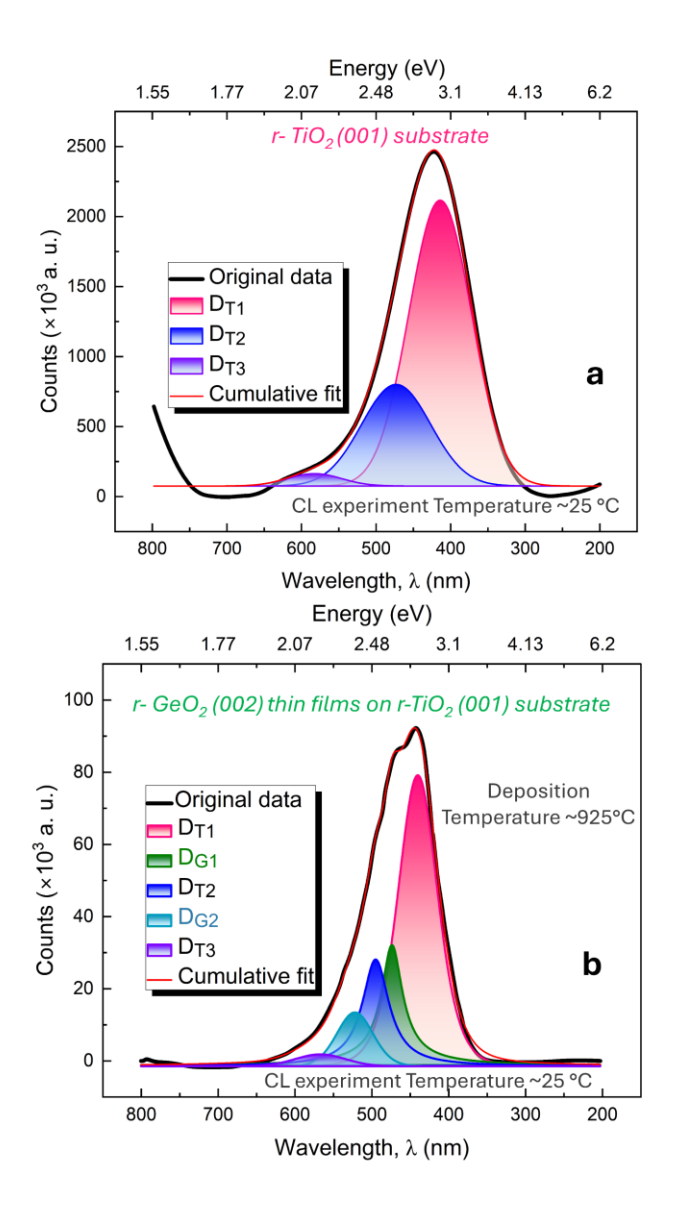


FIG. 3. (a) CL spectrum of bare r-TiO₂ substrate at room temperature, (a) CL spectrum of r-GeO₂ film grown on r-TiO₂ (001).

Similar features have been reported in photoluminescence studies under UV excitation, particularly in undoped r-GeO₂. The overall broadness of the emission spectra and presence of multiple overlapping Gaussian components reflect the complex defect landscape in both the film and substrate. The relative intensity and spectral position of the D_{G1} and D_{G2} peaks suggest potential for tuning the optical behavior of r-GeO₂ through controlled growth conditions and defect engineering. The absence of near-band-edge emission further underscores the dominant influence of intrinsic defects in governing optical characteristics at room temperature.²

Figure 4 presents the XPS analysis of the MOCVD-grown r-GeO₂ thin film to investigate its elemental composition, chemical bonding states, and electronic structure. The survey spectrum shown in Figure 4a reveals prominent photoelectron peaks corresponding to Ge and O, including Ge 3d, Ge 3p_{1/2}, Ge 3s, O 1s, and Ge LMM Auger lines. The absence of extraneous peaks from contaminants or adventitious elements confirms the high chemical purity of the film. A highresolution scan of the Ge 3d core level in Figure 4b exhibits a symmetric peak centered at ~31.8 eV, characteristic of Ge⁴⁺ in GeO₂. The O 1s core level, shown in **Figure 4c**, is deconvoluted into two distinct components: a dominant lattice oxygen peak at ~530.55 eV (L₁) and a weaker shoulder (L₂) at higher binding energy attributed to surface-bound species or oxygen-related defect states. The relative intensity of the lattice oxygen peak further supports the high degree of stoichiometry in the r-GeO₂ film. Figure 4d illustrates the secondary electron cutoff and valence band edge region, used to estimate the valence band maximum (VBM) and the optical bandgap. From the energy difference between the cutoff (~4.75 eV) and the Fermi level, the optical bandgap of the r-GeO₂ film is estimated to be ~4.75 eV. This value is in good agreement with both theoretical predictions and experimental observations for rutile-phase GeO2 films and is

comparable to bandgap estimations derived from energy-loss features in the O 1s and Ge 3d spectra reported in prior studies $^{40-42}$.

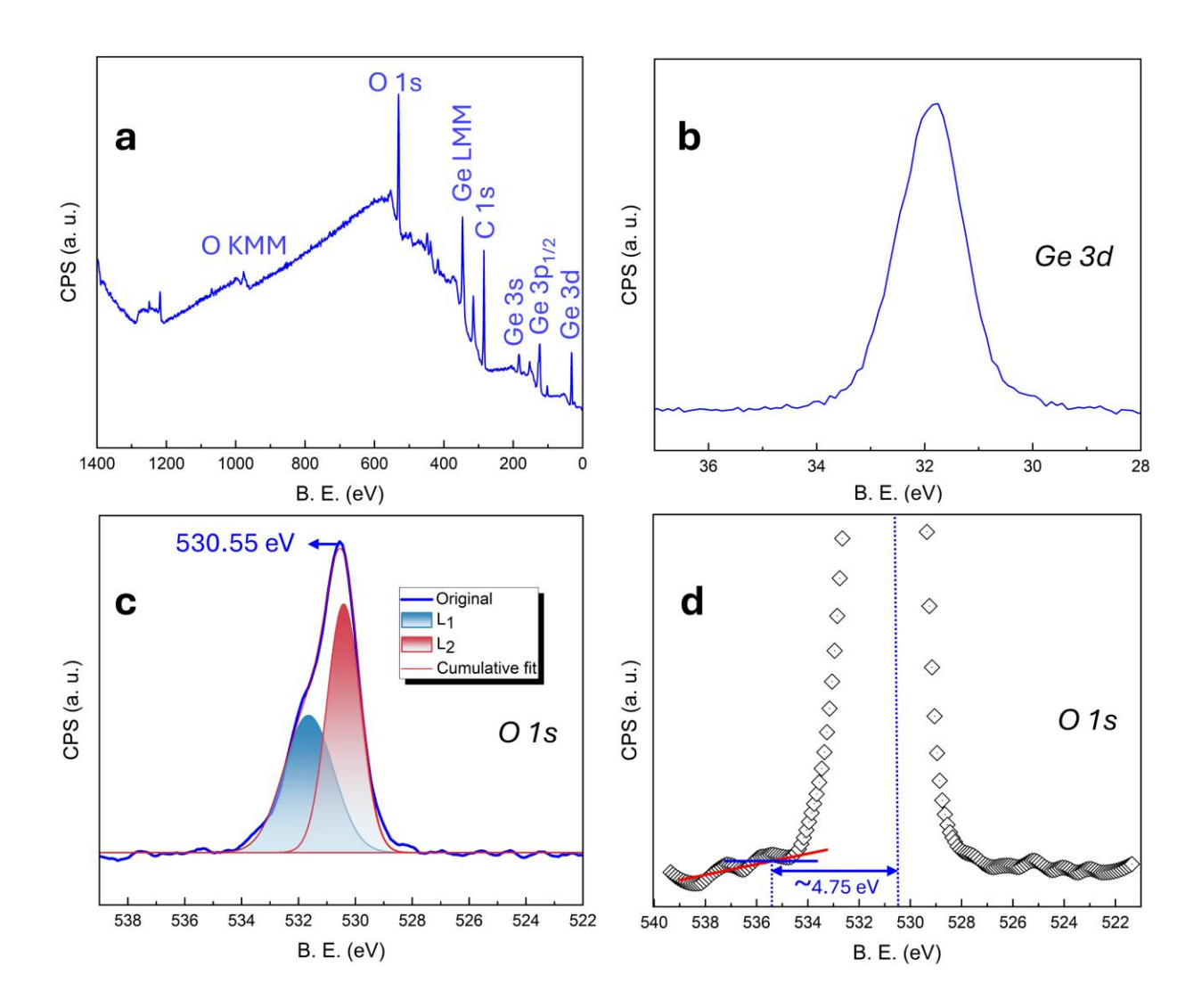


FIG. 4. XPS analysis of r-GeO₂ films. (a) Survey scan confirming the presence of Ge and O without major contamination. (b) Ge 3d peak centered at ~31.8 eV, consistent with Ge⁴⁺. (c) Deconvoluted O 1s peak with a dominant component at 530.55 eV and a secondary peak from defect-related states. (d) Valence band spectrum showing a bandgap of ~4.75 eV estimated from the O 1s cutoff.

Figure 5 illustrates the optical transmittance properties and comparative bandgap benchmarking of MOCVD-grown r-GeO₂ thin films. **Figure 5a** shows the UV–Vis transmittance

spectrum of the r-GeO₂ film, where a steep absorption edge is observed in the 250–260 nm wavelength range, corresponding to an optical bandgap of approximately 4.81–5.0 eV. Although the overall transmittance curve is less defined compared to previously reported UV–Vis spectra of GeO₂ films, this is likely attributed to the faceted surface morphology and relatively high surface roughness of the film and TiO₂ substrate, which can cause increased scattering and light trapping.

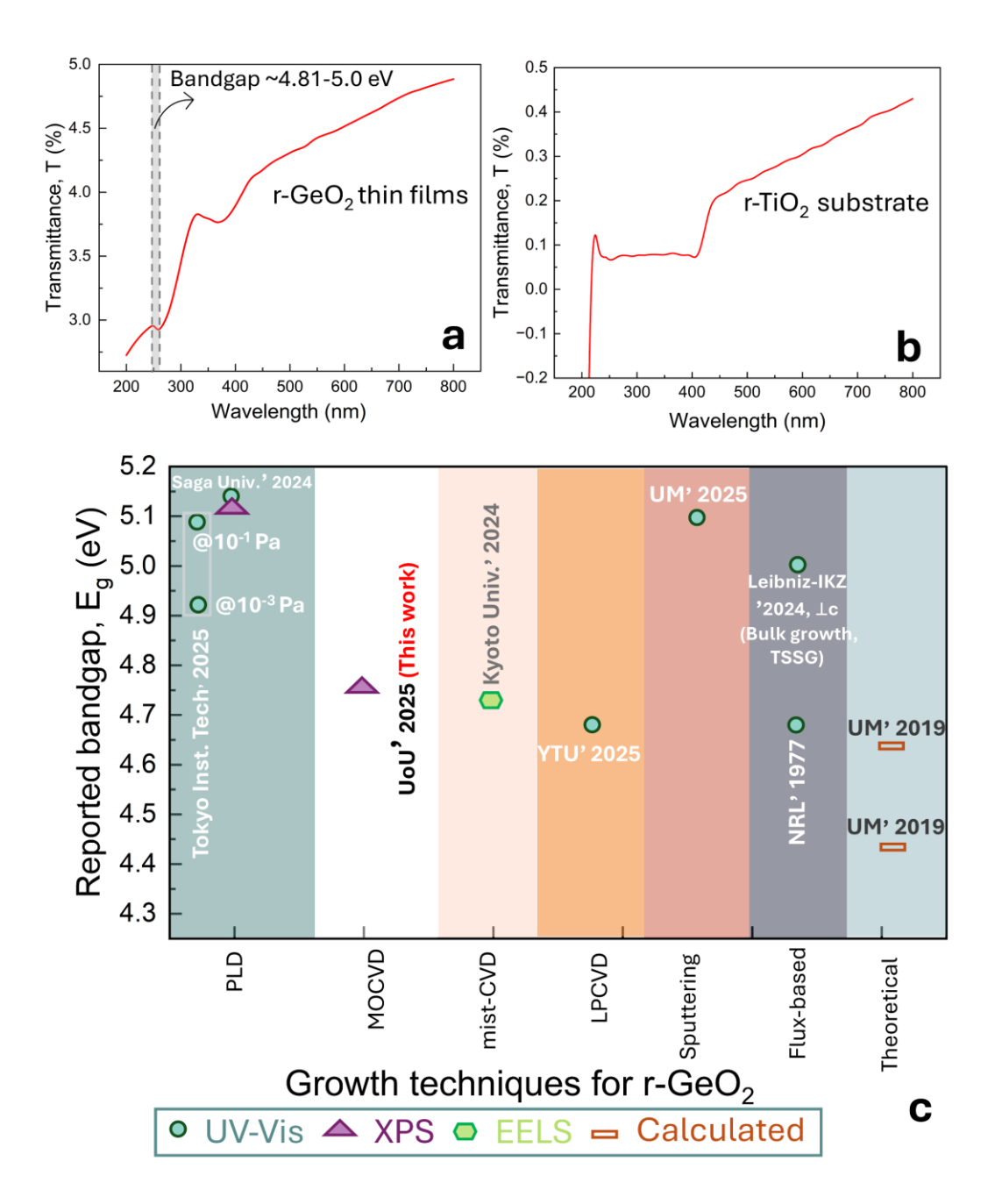


FIG. 5. (a) UV–Vis transmittance spectrum of r-GeO₂ thin films showing a bandgap of ~4.81–5.0 eV. (b) Transmittance spectrum of bare r-TiO₂ substrate for comparison. (c) Reported bandgap values of r-GeO₂ synthesized via different growth techniques and measured using various methods (UV–Vis, XPS, EELS, calculations).

Nevertheless, the absorption edge aligns well with the expected onset for high-quality rutile-phase GeO₂. **Figure 5b** presents the transmittance spectrum of the bare r-TiO₂ (001) substrate, which exhibits notably lower transmittance across the UV–Vis range, confirming that the features seen in **Figure 5a** originate from the overlying r-GeO₂ film. **Figure 5c** benchmarks the bandgap values of r-GeO₂ reported across various deposition methods—including PLD, MOCVD, mist-CVD, LPCVD, sputtering, and bulk flux-based growth (e.g., TSSG)—as well as theoretical predictions. Results by this work (UoU' 2025) are marked with an XPS-derived bandgap of ~4.75 eV, placing it within the expected UWBG regime. The reported values vary from ~4.4 to 5.1 eV, depending on both the growth technique and the method of bandgap extraction (UV-Vis, XPS, EELS, or DFT-based calculations). This comparative overview demonstrates that the optical performance of the present r-GeO₂ films is in strong agreement with established results, validating the quality of the material despite minor spectral deviations due to surface morphology.

This work presents an in-depth investigation into the optical properties of rutile-phase GeO₂ thin films grown on r-TiO₂ (001) substrates via MOCVD. CL spectroscopy reveals broad visible emissions from the r-GeO₂ films, with dominant peaks at 2.64 eV (~470 nm) and 2.38 eV (~520 nm), attributed to excitonic recombination and oxygen-vacancy-related defect centers.² CL mapping further reveals spatially heterogeneous luminescence linked to microstructural variations across the film surface. Regions with larger faceted crystalline domains exhibit more intense CL emissions, while areas composed of smaller or poorly defined crystalline domains show

suppressed luminescence, highlighting the impact of crystalline domain size on optical quality. XPS confirms the presence of Ge⁴⁺ oxidation states through a Ge 3d peak at ~31.8 eV, and lattice oxygen through an O 1s peak at ~530.55 eV. The secondary electron cutoff and valence band edge yield an XPS-derived bandgap of ~4.75 eV. Complementary UV–Vis transmittance measurements show a distinct absorption edge between 250–260 nm, corresponding to an optical bandgap of approximately 4.81–5.0 eV. A benchmarking comparison of bandgap values reported across diverse synthesis methods—including PLD, mist-CVD, LPCVD, sputtering, and TSSG—places the results of this study within the upper range of expected values, underscoring the high optical quality of MOCVD-grown r-GeO₂. Together, these findings advance the understanding of the intrinsic and defect-related optical behavior of r-GeO₂ and support its potential as a compelling ultra-wide bandgap semiconductor for future deep-UV optoelectronics and power device applications.

AUTHOR DECLARATIONS

Conflict of Interest

The authors have no conflicts to disclose.

Author Contributions

Imteaz Rahaman: Data curation (lead); Formal analysis (lead); Investigation (lead); Methodology (lead), Writing-original draft (lead); Anthony Bolda: Data curation (supporting); Botong Li: Writing – review & editing (supporting). Hunter D. Ellis: Writing – review & editing (supporting); Brian Roy Van Devener: Data curation (equal); Writing – review & editing (supporting); Formal analysis (supporting). Kai Fu: Conceptualization (lead); Supervision (lead); Project administration (lead); Resources (lead), Writing – review & editing (lead).

ACKNOWLEDGEMENT

The authors acknowledge the support from the University of Utah start-up fund. This work made use of the Nanofab EMSAL shared facilities of the Micron Technology Foundation Inc. Microscopy Suite, sponsored by the John and Marcia Price College of Engineering, Health Sciences Center, Office of the Vice President for Research. In addition, it utilized the University of Utah Nanofab shared facilities, which are supported in part by the MRSEC Program of the NSF under Award No. DMR-112125.

DATA AVAILABILITY

The data that support the findings of this study are available from the corresponding authors upon reasonable request.

REFERENCES

- ¹ S. Fujita, "Wide-bandgap semiconductor materials: For their full bloom," Jpn. J. Appl. Phys. **54**(3), 030101 (2015).
- ² Z. Galazka, R. Blukis, A. Fiedler, S. Bin Anooz, J. Zhang, M. Albrecht, T. Remmele, T. Schulz, D. Klimm, M. Pietsch, A. Kwasniewski, A. Dittmar, S. Ganschow, U. Juda, K. Stolze, M. Suendermann, T. Schroeder, and M. Bickermann, "Bulk Single Crystals and Physical Properties of Rutile GeO₂ for High-Power Electronics and Deep-Ultraviolet Optoelectronics," Physica Status Solidi (b), (2024).
- ³ J.Y. Tsao, S. Chowdhury, M.A. Hollis, D. Jena, N.M. Johnson, K.A. Jones, R.J. Kaplar, S. Rajan, C.G. Van De Walle, E. Bellotti, C.L. Chua, R. Collazo, M.E. Coltrin, J.A. Cooper, K.R. Evans, S. Graham, T.A. Grotjohn, E.R. Heller, M. Higashiwaki, M.S. Islam, P.W. Juodawlkis, M.A. Khan, A.D. Koehler, J.H. Leach, U.K. Mishra, R.J. Nemanich, R.C.N. Pilawa-Podgurski, J.B. Shealy, Z. Sitar, M.J. Tadjer, A.F. Witulski, M. Wraback, and J.A. Simmons, "Ultrawide-Bandgap

- Semiconductors: Research Opportunities and Challenges," Adv Elect Materials 4(1), 1600501 (2018).
- ⁴ M. Higashiwaki, K. Sasaki, A. Kuramata, T. Masui, and S. Yamakoshi, "Gallium oxide (Ga2O3) metal-semiconductor field-effect transistors on single-crystal β-Ga2O3 (010) substrates," Applied Physics Letters **100**(1), 013504 (2012).
- ⁵ M. Higashiwaki, K. Sasaki, T. Kamimura, M. Hoi Wong, D. Krishnamurthy, A. Kuramata, T. Masui, and S. Yamakoshi, "Depletion-mode Ga2O3 metal-oxide-semiconductor field-effect transistors on β-Ga2O3 (010) substrates and temperature dependence of their device characteristics," Applied Physics Letters **103**(12), 123511 (2013).
- ⁶ M. Oda, R. Tokuda, H. Kambara, T. Tanikawa, T. Sasaki, and T. Hitora, "Schottky barrier diodes of corundum-structured gallium oxide showing on-resistance of 0.1 mΩ·cm ² grown by MIST EPITAXY [®]," Appl. Phys. Express **9**(2), 021101 (2016).
- ⁷ M. Kasu, N.C. Saha, T. Oishi, and S.-W. Kim, "Fabrication of diamond modulation-doped FETs by NO ₂ delta doping in an Al ₂ O ₃ gate layer," Appl. Phys. Express **14**(5), 051004 (2021).
- ⁸ I. Rahaman, H.D. Ellis, C. Chang, D.H. Mudiyanselage, M. Xu, B. Da, H. Fu, Y. Zhao, and K. Fu, "Epitaxial Growth of Ga2O3: A Review," Materials **17**(17), 4261 (2024).
- ⁹ I. Rahaman, H.D. Ellis, B. Li, M. Mohammadi, Y. Wang, and K. Fu, "Investigation of Diamond/Ga2O3 and Diamond/GaN Hetero-p-n Junctions Using Mechanical Grafting," Semicond. Sci. Technol., (2025).
- ¹⁰ D. Wang, H.D. Ellis, D.H. Mudiyanselage, Z. He, B. Da, I. Rahaman, I. Baranowski, S. Gangwal, D. Vasileska, K. Fu, and H. Fu, "Multi-kV AlGaN/GaN Heterojunction Schottky Barrier Diodes with Hydrogen Plasma Guard Array Termination," IEEE Electron Device Lett., 1–1 (2025).
- ¹¹ L. Aborah Yeboah, A. Abdul Malik, P. Agyemang Oppong, P. Sarfo Acheampong, J. Arko Morgan, R. Akua Adwubi Addo, B. Williams Henyo, S. Takyi Taylor, W. Makafui Zudor, and S. Osei-Amponsah, "Wide-Bandgap Semiconductors: A Critical Analysis of GaN, SiC, AlGaN, Diamond, and Ga2O3 Synthesis Methods, Challenges, and Prospective Technological Innovations," Intelligent and Sustainable Manufacturing **2**(1), 10011–10011 (2025).

¹²Gallium Oxide (Elsevier, 2019).

¹³ M. Higashiwaki, and S. Fujita, editors, *Gallium Oxide: Materials Properties, Crystal Growth, and Devices* (Springer International Publishing, Cham, 2020).

- ¹⁴ G.T. Dang, Y. Tagashira, T. Yasuoka, L. Liu, and T. Kawaharamura, "Conductive Si-doped α-(AlxGa1-x)2O3 thin films with the bandgaps up to 6.22 eV," AIP Advances **10**(11), (2020).
- 15 Z. Galazka, S. Ganschow, P. Seyidov, K. Irmscher, M. Pietsch, T.-S. Chou, S. Bin Anooz, R. Grueneberg, A. Popp, A. Dittmar, A. Kwasniewski, M. Suendermann, D. Klimm, T. Straubinger, T. Schroeder, and M. Bickermann, "Two inch diameter, highly conducting bulk β -Ga2O3 single crystals grown by the Czochralski method," Applied Physics Letters **120**(15), (2022).
- ¹⁶ Z. Galazka, D. Klimm, K. Irmscher, R. Uecker, M. Pietsch, R. Bertram, M. Naumann, M. Albrecht, A. Kwasniewski, R. Schewski, and M. Bickermann, "MgGa₂O₄ as a new wide bandgap transparent semiconducting oxide: growth and properties of bulk single crystals," Phys. Status Solidi A **212**(7), 1455–1460 (2015).
- ¹⁷ Z. Galazka, S. Ganschow, R. Schewski, K. Irmscher, D. Klimm, A. Kwasniewski, M. Pietsch, A. Fiedler, I. Schulze-Jonack, M. Albrecht, T. Schröder, and M. Bickermann, "Ultra-wide bandgap, conductive, high mobility, and high quality melt-grown bulk ZnGa2O4 single crystals," APL Materials 7(2), (2019).
- ¹⁸ I.H. Emu, B.C. Samuels, S. Karmakar, M.A. Hamid, I.F. Shiam, P.K. Sarkar, A. Tasnim, A. Haque, and R. Droopad, "Epitaxial growth and characterization of copper gallate (CuGa2O4) thin films by pulsed laser deposition," Materials Science in Semiconductor Processing **185**, 108934 (2025).
- ¹⁹ S. Chae, K. Mengle, K. Bushick, J. Lee, N. Sanders, Z. Deng, Z. Mi, P.F.P. Poudeu, H. Paik, J.T. Heron, and E. Kioupakis, "Toward the predictive discovery of ambipolarly dopable ultra-wide-band-gap semiconductors: The case of rutile GeO2," Applied Physics Letters **118**(26), 260501 (2021).
- ²⁰ C.A. Niedermeier, K. Ide, T. Katase, H. Hosono, and T. Kamiya, "Shallow Valence Band of Rutile GeO ₂ and P-type Doping," J. Phys. Chem. C **124**(47), 25721–25728 (2020).
- ²¹ G. Deng, K. Saito, T. Tanaka, M. Arita, and Q. Guo, "Pulsed laser deposition growth of ultrawide bandgap GeO2 film and its optical properties," Applied Physics Letters **119**(18), 182101 (2021).
- ²² K. Bushick, K.A. Mengle, S. Chae, and E. Kioupakis, "Electron and hole mobility of rutile GeO2 from first principles: An ultrawide-bandgap semiconductor for power electronics," Applied Physics Letters **117**(18), 182104 (2020).

- ²³ I. Rahaman, B.G. Duersch, H.D. Ellis, M.A. Scarpulla, and K. Fu, "Epitaxial growth of rutile GeO2 via MOCVD," Applied Physics Letters **125**(10), 102103 (2024).
- ²⁴ S. Chae, K.A. Mengle, R. Lu, A. Olvera, N. Sanders, J. Lee, P.F.P. Poudeu, J.T. Heron, and E. Kioupakis, "Thermal conductivity of rutile germanium dioxide," Applied Physics Letters **117**(10), 102106 (2020).
- ²⁵ J.L. Lyons, and A. Janotti, "A p-type dopable ultrawide-bandgap oxide," J. Phys.: Condens. Matter **36**(8), 085501 (2024).
- ²⁶ M. Stapelbroek, and B.D. Evans, "Exciton structure in the u.v.-absorption edge of tetragonal GeO2," Solid State Communications **25**(11), 959–962 (1978).
- ²⁷ G. Deng, Y. Huang, Z. Chen, K. Saito, T. Tanaka, M. Arita, and Q. Guo, "Heteroepitaxy of (1 0 0)-oriented rutile GeO2 film on c-plane sapphire by pulsed laser deposition," Materials Letters **326**, 132945 (2022).
- ²⁸ G. Deng, Y. Huang, Z. Chen, K. Saito, T. Tanaka, M. Arita, and Q. Guo, "Temperature-dependent photoluminescence of r-GeO2 film deposited on r-plane sapphire by synchrotron radiation excitation," Journal of Luminescence **267**, 120353 (2024).
- ²⁹ H. Takane, and K. Kaneko, "Establishment of a growth route of crystallized rutile GeO2 thin film ($\ge 1 \mu$ m/h) and its structural properties," Applied Physics Letters **119**(6), 062104 (2021).
- ³⁰ Y. Li, W. Yin, R. Deng, R. Chen, J. Chen, Q. Yan, B. Yao, H. Sun, S.-H. Wei, and T. Wu, "Realizing a SnO2-based ultraviolet light-emitting diode via breaking the dipole-forbidden rule," NPG Asia Mater 4(11), e30–e30 (2012).
- ³¹ S. Chae, H. Paik, N.M. Vu, E. Kioupakis, and J.T. Heron, "Epitaxial stabilization of rutile germanium oxide thin film by molecular beam epitaxy," Applied Physics Letters **117**(7), 072105 (2020).
- ³² S.L. Shinde, and K.K. Nanda, "Thermal oxidation strategy for the synthesis of phase-controlled GeO₂and photoluminescence characterization," CrystEngComm **15**(6), 1043–1046 (2013).
- ³³ A. Trukhin, M. Kink, Y. Maksimov, J. Jansons, and R. Kink, "Luminescence of GeO2 glass, rutile-like and α-quartz-like crystals," Journal of Non-Crystalline Solids **352**(2), 160–166 (2006).
- ³⁴ S. Chae, L.A. Pressley, H. Paik, J. Gim, D. Werder, B.H. Goodge, L.F. Kourkoutis, R. Hovden, T.M. McQueen, E. Kioupakis, and J.T. Heron, "Germanium dioxide: A new rutile substrate for epitaxial film growth," Journal of Vacuum Science & Technology A **40**(5), 050401 (2022).

- ³⁵ I. Rahaman, B. Li, B.G. Duersch, H.D. Ellis, and K. Fu, "Seed-Driven Stepwise Crystallization (SDSC) for Growing Rutile GeO₂ Films via MOCVD," ACS Appl. Electron. Mater., acsaelm.4c02361 (2025).
- ³⁶ N.D. Abazović, M.I. Čomor, M.D. Dramićanin, D.J. Jovanović, S.P. Ahrenkiel, and J.M. Nedeljković, "Photoluminescence of Anatase and Rutile TiO₂ Particles," J. Phys. Chem. B **110**(50), 25366–25370 (2006).
- ³⁷ D.K. Pallotti, L. Passoni, P. Maddalena, F. Di Fonzo, and S. Lettieri, "Photoluminescence Mechanisms in Anatase and Rutile TiO₂," J. Phys. Chem. C **121**(16), 9011–9021 (2017).
- ³⁸ M.S. Rathore, A. Vinod, R. Angalakurthi, A.P. Pathak, F. Singh, S.K. Thatikonda, and S.R. Nelamarri, "Ion beam modification of structural and optical properties of GeO2 thin films deposited at various substrate temperatures using pulsed laser deposition," Appl. Phys. A **123**(11), 708 (2017).
- ³⁹ M.S. Rathore, A. Vinod, R. Angalakurthi, A.P. Pathak, S.K. Thatikonda, and S.R. Nelamarri, "Role of oxygen pressure on the structural and photoluminescence properties of pulsed laser deposited GeO2 thin films," Physica B: Condensed Matter **625**, 413466 (2022).
- ⁴⁰ H. Takane, S. Konishi, R. Ota, Y. Hayasaka, T. Wakamatsu, Y. Isobe, K. Kaneko, and K. Tanaka, "Transmission electron microscopic study on rutile-type GeO2 film on TiO2 (001) substrate," Applied Physics Letters **125**(21), 212102 (2024).
- 41 F. Golbasi, B. Liu, J. Hwang, and F. Akyol, "Characteristics of Single Crystalline Rutile Ge O 2 Film Grown on Sapphire by Chemical Vapor Deposition with a high growth rate ~2.2 μ m/hr," Journal of Alloys and Compounds **1014**, 178591 (2025).
- ⁴² S. Chae, J. Lee, K.A. Mengle, J.T. Heron, and E. Kioupakis, "Rutile GeO2: An ultrawide-band-gap semiconductor with ambipolar doping," Applied Physics Letters **114**(10), 102104 (2019).